Study on the vorticity field within the tail reconnection jet by the MMS spacecraft

L. Q. Zhang[1], W. Baumjohann[2], L. Wang[3], C. Wang[1], Y. Ren[1], James L. Burch[4], Yu. V. Khotyaintsev[5], J. Y. Wang[6]

1. State Key Laboratory of Space Weather (National Space Science Center, Chinese Academy of Sciences), Beijing, 100080, China (e-mail: lqzhang@nssc.ac.cn)
2. Space Research Institute, Austrian Academy of Sciences, 8042 Graz, Austria
3. Department of Astrophysical Sciences, Princeton University, Princeton, NJ, USA
4. Southwest Research Institute San Antonio, San Antonio, TX 78238, USA
5. Swedish Institute of Space Physics, Uppsala, Sweden
6. Information Engineering College, Central University for Nationalities, Beijing, 100081, China

Key points:

1) Within the reconnection jet, also named bursty bulk flow (BBF), the vorticity field (**ω**) and jet velocity are highly correlated: the higher **V**, the stronger **ω**.
2) The BBF **ω**-field is dominated by the perpendicular vorticity.
3) Concerning β-dependence, the **ω**-field tends to be stronger in super-M_A jet than in sub-M_A jet.

Abstract Based on direct measurement by the MMS spacecraft in the years of 2017 and 2018, we perform studies on the vorticity field (**ω**) within the reconnection jet in the plasma sheet. A typical event on 26 July 2017 shows clearly the evolution of the **ω**-field with the jet velocity: **ω** is weak in the decelerated BBF and strong in the fast BBF. The strongest **ω**-field is in the decaying BBF, around the dipolarization fronts. Despite the evolution of the BBF, the **ω**-field is characterized by the perpendicular vorticity ($\omega_{\perp}$). Statistical results confirm the close correlation between BBF **V** and **ω**. Higher **V** means stronger **ω**. This accounts for the dawn-dusk asymmetry of the **ω**-field. The anisotropic is more significant in the $V_{\perp}$-dominating BBF than in the $V_{//}$-dominating BBF. The **ω**-field within the reconnection jet is β-dependence. The β-dependence **ω**-field tends to be stronger in super-M_A jet than in sub-M_A jet.

1. Introduction

A reconnection jet, also named BBF, is the most significant and common phenomenon in the Earth's magnetotail [e.g., Angelopoulos et al., 1992; 1994; Baumjohann et al., 1988; 1989; 1990; Zhang et al., 2009; 2010; 2015a,b; 2016a, b]. It provides the main task of the mass, energy, and magnetic flux transport in the tail plasma sheet. A BBF drives serious activities in the magnetosphere and ionosphere [Angelopoulos et al., 2008], by releasing its energy locally in the down-tail region [e.g., Zhang et al., 2020] and/or globally in the near-Earth braking region [Shiokawa, 1997; Shiokawa et al., 1998].

The BBF is inherently a highly turbulent flow, both in its velocity field [e.g., Borovsky et al., 1997; Borovsky and Bonnel, 2001; Borovsky et al., 2003; Zhang et al.,

2019] and in the E/B field [e.g., Tu et al, 2000; Angelopoulos et al., 2002; Wygant et al., 2005; Dai et al., 2011; 2017; Zelenyi et al., 2014; Stawarz et al., 2015]. The kinetic Alfvénic wave (KAW) has been invoked to interpret the E/B turbulence in the course of the BBF. The KAW, including its strength and scaling, depends highly on the flow velocity [Vörös et al., 2004; 2006; Zimbardo, et al., 2010; Chaston et al., 2008; 2012].

The vorticity field ($\boldsymbol{\omega} = \nabla \times \mathbf{V}$) carries the essential information of the turbulence in fluids. Recently, utilizing four-point measurement from the Magnetospheric Multiscale (MMS) spacecraft, Zhang et al. [2019] analyzed the plasma vorticity within a BBF. Their result demonstrates the enhanced vorticity in the course of the BBF. Increase of the vorticity is associated with enhancements of the high-energy ion flux (above 10 keV) and the enhancement of the current **J**. A new scenario of the superposition of the eddy and KAW turbulence is proposed to interpret the BBF turbulence.

Till now, a statistical study on the properties of the vorticity field within the reconnection jet is still lacking. In this paper, we present the first statistical result on the **ω**-field of the BBF based on direct four-point measurement by MMS spacecraft in the tail seasons of 2017 and 2018. Case study and statistical result show clearly the correlation between BBF velocity **V** and vorticity **ω**. Besides, the **ω**-field within the reconnection jet depends highly on plasma β and the Alfvénic March number ($M_A=V/V_A$). MMS observation suggests the significance of the embedded current sheet on the BBF **ω**-field.

2. Data description

MMS operates in the magnetotail from May to Oct in the year of 2017 and 2018, with the apogee of 24.5 R_E. The 0.125-s resolution data of fluxgate magnetometers (FGM)

[Russell et al., 2016; Torbert et al., 2016], 0.03-s resolution of Electric Field Instrument (EDP [Lindqvist et al., 2014] and 4.5-s data of Fast Plasma Investigation (FPI) [Pollock et al., 2016] on four MMS satellites during this interval are collected.

The burst flows are selected by the criterion of the duration of V_x > 300 km/s for longer than 15 s. The selection region is confined in the box of -25 R_E < X < -7 R_E, -15 R_E < Y < 15 R_E and -5 R_E < Z < 5 R_E (GSM coordinates). There are totally 759 bursty flows recorded by MMS. For each event, the curlometer method is applied to calculate the vorticity ($\boldsymbol{\omega} = \nabla \times \mathbf{V}$) [Zhang et al., 2019].

3. Typical events

On 27 July 2017 from 17:15 to 17:50 UT, MMS1 locates near the neutral sheet around (-23.4 R_E, 6.4 R_E, 4.4 R_E) and records the continuous BBF. Overview of the temporal evolutions of the field and plasma during the same interval are shown in Figure 1. The BBF lasts from17: 22 UT (first solid vertical line) to 17:39 UT (last black dashed vertical line), characterized by the finger-like structures of the ion energy spectra [Zhang et al., 2019; 2020]. The ion temperature is higher during the BBF interval. The average Alfvénic velocity ($V_A = B_0/\sqrt{4\pi\rho}$) is 267 km/s.

The BBF experiences three different stages, including weak-BBF, strong-BBF, and decaying-BBF. The average velocity of the weak-BBF is only ~200 km/s, lower than V_A. At 17:31 UT (marked by the first black dashed line), the BBF is suddenly enhanced. The strong-BBF has significant parallel component ($V_{//}$). After 17:35 UT (marked by the yellow dashed line), the BBF rapidly decays. In the decaying-BBF, the Vy is strong.

Before and after the BBF, the Bz component in the background plasma sheet is increased from 0.2 nT to 5 nT. The magnetic field in Panels D and E has slowly large-amplitude fluctuation in the weak-BBF, and rapidly small-amplitude in the strong-BBF. Accompanying with the magnetic field fluctuations, the ion density fluctuates also. In the decaying-BBF, two dipolarization fronts (DFs) emerge, signed by the sharp Bz-enhancement and the simultaneous B_T-enhancement. As a contrast, the ion temperature dips at the DFs.

Evolutions of three components of the vorticity field are presented in Panels H to J. The ω has substantial enhancement in the course of the BBF. The ω_z is generally the main component. The ω_y becomes significant in the decaying-BBF. Despite the evolution of the BBF, the $\omega_\perp$ is the dominant component (Panel K). The anisotropic angle ($\theta_{AA} = \arctan(\frac{\omega_\perp}{\omega_{//}})$) is averagely 65.3°. Apparently, the **ω**-field is characterized by the perpendicular-predominantly vorticity

4. Statistical study

Dawn-dusk asymmetry

The BBFs are classified into two groups according to their angels between V and B ($\theta_{VB} = \arctan(\frac{V_\perp}{V_{//}})$), i.e., $V_{//}$-dominating BBF ($\theta_{VB} < 45°$) and $V_\perp$-dominating BBF ($\theta_{VB} > 45°$). The BBF ω and other parameters are the average value in the course of the BBF.

Evolutions of the ω field in the dawn-dusk direction for the $V_{//}$-dominating BBF and $V_\perp$-dominating BBF are shown in Figure 2. The ω-field in Panels B and C has significant

dawn-dusk asymmetry. As a whole, the BBF ω is stronger in the dawn side than in the dusk side.

The BBF Vx is shown in Panel A. We can see that the BBF V and ω are highly correlated. Higher **V** means stronger **ω**. Similar dawn-dusk asymmetry can be seen in the BBF Vx. This accounts for the dawn-dusk asymmetry of the ω-field.

Anisotropy

Histogram of probabilities of the θ_{AA} of the BBF is shown in Figure 3. The $V_{//}$-dominating and $V_{\perp}$-dominating BBF have similar distributions. Both have almost symmetric distributions. Both BBFs occur mostly for $|\theta_{AA}| > 60°$. Statistically, the BBF vorticity is $\omega_{\perp}$-dominating. Relatively, the perpendicular BBF have higher $|\theta_{AA}|$ than the parallel BBF. The anisotropy is more significant in the perpendicular BBF than in the parallel BBF.

β-dependence

Scatter plot of β versus ω is presented in Figure 4. It can be seen that the small-ω field ($\omega < 1$) dominates the regime of $\beta < 200$ while the large-ω field ($\omega > 1$) dominates the regime of $\beta > 200$. As we have known, magnetic Prandtl number ($Pm=\mu_0\sigma\mu$) is an increasing function of the plasma beta value. It can be inferred that within the reconnection jet, the ω-field is stronger/weaker in the regime of higher/lower Pm (magnetic Prandtl number $Pm=\mu_0\sigma\mu$).

The colored M_A of the BBF is also presented in Figure 4. Clearly, the reconnection jet could be super-M_A as well as sub-M_A as well. Note that seldom small-ω BBF occurs for $M_A > 1.5$ ($\beta > 1000$). It appears that the β-dependence **ω**-field tends to be stronger in super-M_A jet than in sub-M_A jet.

5. Discussion

A cartoon illustration of the vorticity field within the earthward traveling BBF embedded unsteady current sheet is shown in Figure 5. In the equatorial region (X-Y plane), the ω_z is the dominant component. The ω-field is stronger on the dawn side than on the dusk side.

Previous studies showed that the plasma ω of the KAW is nearly field-aligned [Phan et al., 2016; Hwang et al., 2019; Wang et al., 2019]. This agrees with the perpendicular-cascade of the KAW turbulence. Unlike the KAW-vorticity, the BBF-vorticity is predominantly perpendicular. The $\omega_\perp$-dominating vorticity could introduce parallel cascade in the BBF turbulence.

The β-dependence and anisotropic strongly suggests the significance of the embedded current sheet on the **ω**-field of the reconnection jet. This current sheet determines the magnetic structure in the normal direction within the reconnection jet [Nakamura et al., 2006; 2008], hence, the plasma β and the flow structure with respect to the magnetic field (parallel or perpendicular) [Zhang et al., 2010a].

Interaction between the embedded current sheet and the BBF could have substantial influence on the evolution of the **ω**-field. The thin current sheet facilitates the K-H wave/instability [e.g., Horton et al., 1987; Dai, 2009, Dai et al., 2011]. It can be expected the generation of the K-H vortex within the reconnection jet [Turkakin et al., 2014]. On the other hand, emitting KAW by unstable current sheet (kink and/or tear) dissipates the kinetic energy of the BBF [Hoshino and Higashimori, 2015]. This may lead to the decay of the vorticity field.

6. Conclusions

As a conclusion, the BBF **V** and **ω** are highly correlated. Higher **V** means stronger **ω** is. The **ω**-field within the reconnection jet is characterized by the perpendicular-predominantly component. The anisotropic, quantified by the anisotropic angle ($\theta_{AA} = \arctan(\frac{\omega_{\perp}}{\omega_{//}})$), is more significant in the $V_{\perp}$-dominating BBF than in the $V_{//}$-dominating BBF. Besides, the BBF **ω** is β-dependence. The β-dependence **ω**-field tends to be stronger in super-M_A jet than in sub-M_A jet. MMS result highlights the potential significance of the embedded current sheet on the **ω**-field in the course of the BBF.

Acknowledgements We would like to thank the PIs and those who contributed to the success of the MMS mission. The data of MMS satellite is available from: https://cdaweb.gsfc.nasa.gov/pub/data/mms/. This study is supported by the National Natural Science Foundation of China (41774177) and in part by the specialized research fund for state key laboratories and the strategic pioneer program on space science II, Chinese Academy of Sciences, Grant No. XDA15350201 and XDA15011401.

References

1. Angelopoulos, V., W. Baumjohann, C. F. Kennel, F. V. Coroniti, M. G. Kivelson, R. Pellat, R. J. Walker, H. Lühr, and G. Paschmann (1992), Bursty bulk flows in the inner central plasma sheet, *J. Geophys. Res.*, 97(A4), 4027–4039, doi:10.1029/91JA02701.
2. Angelopoulos, V., C. F. Kennel, F. V. Coroniti, R. Pellat, M. G. Kivelson, R. J. Walker, C. T. Russell, W. Baumjohann, W. C. Feldman, and J. T. Gosling (1994), Statistical characteristics of bursty bulk flow events, *J. Geophys. Res.*, 99(A11), 21,257–21,280, doi: 10.1029/94JA01263.
3. Angelopoulos, V., J. A. Chapman, F. S. Mozer, J. D. Scudder, C. T. Russell, K. Tsuruda, T. Mukai, T. J. Hughes, and K. Yumoto (2002), Plasma sheet electromagnetic power generation and its dissipation along auroral field lines, *J. Geophys. Res.*, 107(A8), 1181, doi:10.1029/2001JA900136.
4. Angelopoulos, V., et al. (2008), Tail reconnection triggering substorm onset, *Science.* , 321, 931, doi:10.1126/science.1160495.
5. Baumjohann, W., G. Paschmann, N. Sckopke, C. A. Cattell, and C. W. Carlson (1988), Average ion moments in the plasma sheet boundary layer, J. Geophys. Res., 93, 11,507–11,520, doi:10.1029/JA093iA10p11507.
6. Baumjohann, W., et al. (1989), Average plasma properties in the center plasma sheet. *J. Geophys. Res*, 1989, 94, 6597-6606, doi:10.1029/JA094iA06p06597.

7. Baumjohann, W., et al. (1990), Characteristics of high-speed ion flows in the plasma sheet. *J. Geophys. Res.*, 95, 11507-11520, doi:10.1029/JA095iA04p03801
8. Borovsky, J. E., R. C. Elphic, H. O. Funsten, and M. F. Thomsen (1997), The Earth's plasma sheet as a laboratory for flow turbulence in high-βMHD, *J. Plasma Phys.*, 57, 1, doi:10.1017/S0022377896005259.
9. Borovsky, J. E., and J. Bonnell (2001), The dc electrical coupling of flow vortices and flow channels in the magnetosphere to the resistive ionosphere, J. Geophys. Res., 106(A12), 28967–28994, doi: 10.1029/1999JA000245.
10. Borovsky, J. E., and H. O. Funsten (2003), MHD turbulence in the Earth's plasma sheet: Dynamics, dissipation, and driving, *J. Geophys. Res.*, 108(A7), 1284, doi:10.1029/2002JA009625.
11. Chaston, C. C., C. Salem, J. W. Bonnell, C. W. Carlson, R. E. Ergun, R. J. Strangeway, and J. P. McFadden (2008), The turbulent Alfvénic aurora, *Phys. Rev. Lett.*, 100, 175003, doi:10.1103/PhysRevLett.100.175003.
12. Chaston, C. C., J. W. Bonnell, L. Clausen, and V. Angelopoulos (2012), Correction to "Energy transport by kinetic-scale electromagnetic waves in fast plasma sheet flows", *J. Geophys. Res.*, 117, A12205, doi:10.1029/2012JA018476.
13. Dai, L. (2009), Collisionless Magnetic Reconnection via Alfvén Eigenmodes, *Phys. Rev. Letts*, 102 (24), 245,003-245,013, doi:10.1103/PhysRevLett.102.24500
14. Dai, L., J. R. Wygant, C. Cattell, J. Dombeck, S. Thaller, C. Mouikis, A. Balogh, and H. Rème (2011), Cluster observations of surface waves in the ion jets from magnetotail reconnection, *J. Geophys.* Res., 116, A12227, doi:10.1029/2011JA017004.
15. Dai, L., C. Wang, Y. Zhang, B. Lavraud, J. Burch, C. Pollock, and R. B. Torbert (2017), Kinetic Alfven wave explanation of the Hall fields in magnetic reconnection, Geophys. Res. Lett., 44, 634–640, doi:10.1002/2016GL071044.
16. Horton, W., Tajima, T., & Kamimura, T. (1987). Kelvin-Helmholtz instability and vortices in magnetized plasma. *The Physics of Fluids,* 30(11), 3485-3495. https://doi.org/10.1063/1.866429
17. Hoshino, M., and K. Higashimori (2015), Generation of Alfvénic waves and turbulence in reconnection jets, *J. Geophys. Res., Space Physics*, 120, 3715–3727,doi:10.1002/2014JA020520.
18. Hwang, K.-J., Choi, E., Dokgo, K., Burch, J. L., Sibeck, D. G., Giles, B. L., et al. (2019). Electron vorticity indicative of the electron diffusion region of magnetic reconnection. Geophysical Research Letters, 46, 6287–6296. https://doi.org/10.1029/2019GL082710
19. Nakamura, R., W. Baumjohann, Y. Asano, A. Runov, A. Balogh, C. J. Owen, A. N. Fazakerley, M. Fujimoto, B. Klecker, and H. Rème (2006), Dynamics of thin current sheets associated with magnetotail reconnection, *J. Geophys. Res.*, 111, A11206, doi:10.1029/2006JA011706.
20. Nakamura, R., et al. (2008), Cluster observations of an ion-scale current sheet in the magnetotail under the presence of a guide field, *J. Geophys. Res.*, 113, A07S16, doi:10.1029/2007JA012760.
21. Phan, T. D., et al. (2016), MMS observations of electron-scale filamentary currents in the reconnection exhaust and near the X line, Geophys. Res. Lett., 43, 6060– 6069, doi:10.1002/2016GL069212.

22. Pollock, C., et al. (2016), Fast plasma investigation for magnetosphere multiscale, *Space Sci. Rev.*, *199*, 331–406,doi:10.1007/s11214-016-0245-4.
23. Russell, C. T., et al. (2016), The magnetospheric multiscale magnetometers, *Space Sci. Rev.*, *199*, 189–256, doi:10.1007/sl1214-014-0057-3.
24. Shiokawa, K., et al. (1997), Braking of high-speed flows in the near-Earth tail, *Geophys. Res. Lett.*, 24, 1179-1182, doi:10.1029/97GL01062.
25. Shiokawa, K., Baumjohann, G. Haerendel, G. Paschmann, J. F. Fennell, E. Friis-Christensen, H. Luhr, G. D. Reeves, C. T. Russell, P. R. Sutcliffe, K. Takahashi, (1998), High-speed ion flow, substorm current wedge, and multiple Pi2 pulsations, *J. Geophys. Res.*, 103, 4491-4507. doi:10.1029/1997JA01680
26. Stawarz, J. E., R. E. Ergun, and K. A. Goodrich (2015), Generation of high-frequency electric field activity by turbulence in the Earth's magnetotail, *J. Geophys. Res. Space Physics*, 120, doi:10.1002/2014JA020166.
27. Torbert, R. B., et al. (2016), The FIELDS instrument suite on MMS: Scientific objectives, measurements, and data products, *Space Sci. Rev.*,*199*, 105–135, doi:10.1007/s11214-014-0109-8.
28. Tu, J.-N et al., (2000), Statistical nature of impulsive electric fields associated with fast ion flow in the near-Earth plasma sheet, *J. Geophys. Res.*, 105, 18901-18907, doi:10.1002/1999JA000428.
29. Turkakin, H., Mann, I. R., and Rankin, R. (2014), Kelvin-Helmholtz unstable magnetotail flow channels: Deceleration and radiation of MHD waves, Geophys. Res. Lett., 41, 3691– 3697, doi:10.1002/2014GL060450.
30. Vörös, Z., et al. (2004), Magnetic turbulence in the plasma sheet, J. Geophys. Res., 109, A11215, doi:10.1029/2004JA010404.
31. Vörös, Z., W. Baumjohann, R. Nakamura, M. Volwerk, and A. Runov (2006), Bursty bulk flow driven turbulence in the Earth's plasma sheet, Space Sci. Rev., 122(1–4), 301–311, doi:10.1007/s11214-006-6987-7.
32. Wang, T., Alexandrova, O., Perrone, D., Dunlop, M., Dong, X., Bingham, R., Burch, J. L. (2019). Magnetospheric Multiscale Observation of Kinetic Signatures in the Alfvén Vortex. The Astrophysical Journal, 871(2), L22. doi:10.3847/2041-8213/aafe0d
33. Weygand, J. M., et al. (2005), Plasma sheet turbulence observed by Cluster II, J. Geophys. Res., 110, A01205, doi:10.1029/2004JA010581
34. Zelenyi, L., A. Artemyev, and A. Petrukovich (2014), Properties of magnetic field fluctuations in the Earth's magnetotail and implications for the general problem of structure formation in hot plasmas, *Space Sci. Rev.*, doi:10.1007/s11214-014-0037-7.
35. Zhang, L. Q., et al. (2009), Convective bursty flows in the near-Earth magnetotail inside 13 R_E, *J. Geophys. Res.*, 114, A02202, doi:10.1029/2008JA013125.
36. Zhang, L. Q., Z. X. Liu, Z. W. Ma, W. Baumjohann, Z. Y. Pu, M. W. Dunlop, H. Reme, and J. Y. Wang (2010), X line distribution determined from earthward and tailward convective bursty flows in the central plasma sheet, *J. Geophys. Res.*, 115, A06218, doi:10.1029/2009JA014429.
37. Zhang, L. Q., L.D, W. Baumjohann, H. Rème, M. W. Dunlop, and X. H. Wei (2015a), Parallel-dominant and perpendicular-dominant components of the fast bulk flow: comparing with the PSBL beams, J. *Geophys. Res.*, 120, doi:10.1029/2015JA021669

38. Zhang, L. Q., J. Y. Wang, W. Baumjohann, H. Rème, L. Dai, M. W. Dunlop, T. Chen, and Y. Huang (2015b), X-lines in the magnetotail for southward and northward IMF conditions, *J. Geophys. Res. Space Physics*, doi:10.1002/2015JA021503.
39. Zhang, L. Q., L. Dai, W. Baumjohann, A. T. Y. Lui, C. Wang, H. Rème, and M. W. Dunlop (2016a), Temporal evolutions of the solar wind conditions at 1 AU prior to the near-Earth X-lines in the tail: Superposed epoch analysis, *J. Geophys. Res.*, doi:10.1002/2016JA022687.
40. Zhang, L. Q., A. T. Y. Lui, C. Wang, L. Dai, and B. B. Tang (2016b), Bursty bulk flows at different magnetospheric activity levels: dependence on IMF conditions *J. Geophys. Res.*, 122, doi:10.1029/ 2016JA022397.
41. Zhang, L. Q., Baumjohann, W., Dai, L., Khotyaintsev, Y. V., & Wang, C. (2019). Measurements of the vorticity in the bursty bulk flows. *Geophysical Research Letters*, 46, 10322-10329. https://doi.org/10.1029/2019GL084597
42. Zhang, L. Q. et al. (2020), BBF deceleration down-tail of X <-15 RE from MMS observation, *J. Geophys. Res.*, https://doi.org/10.1029/ 2019JA026837.
43. Zimbardo et al. (2010), Magnetic turbulence in the geospace environment, 156, 89-134, *Space Science Reviews*, 156: 89-134, doi: 10.1007/s11214-010-9692-5.

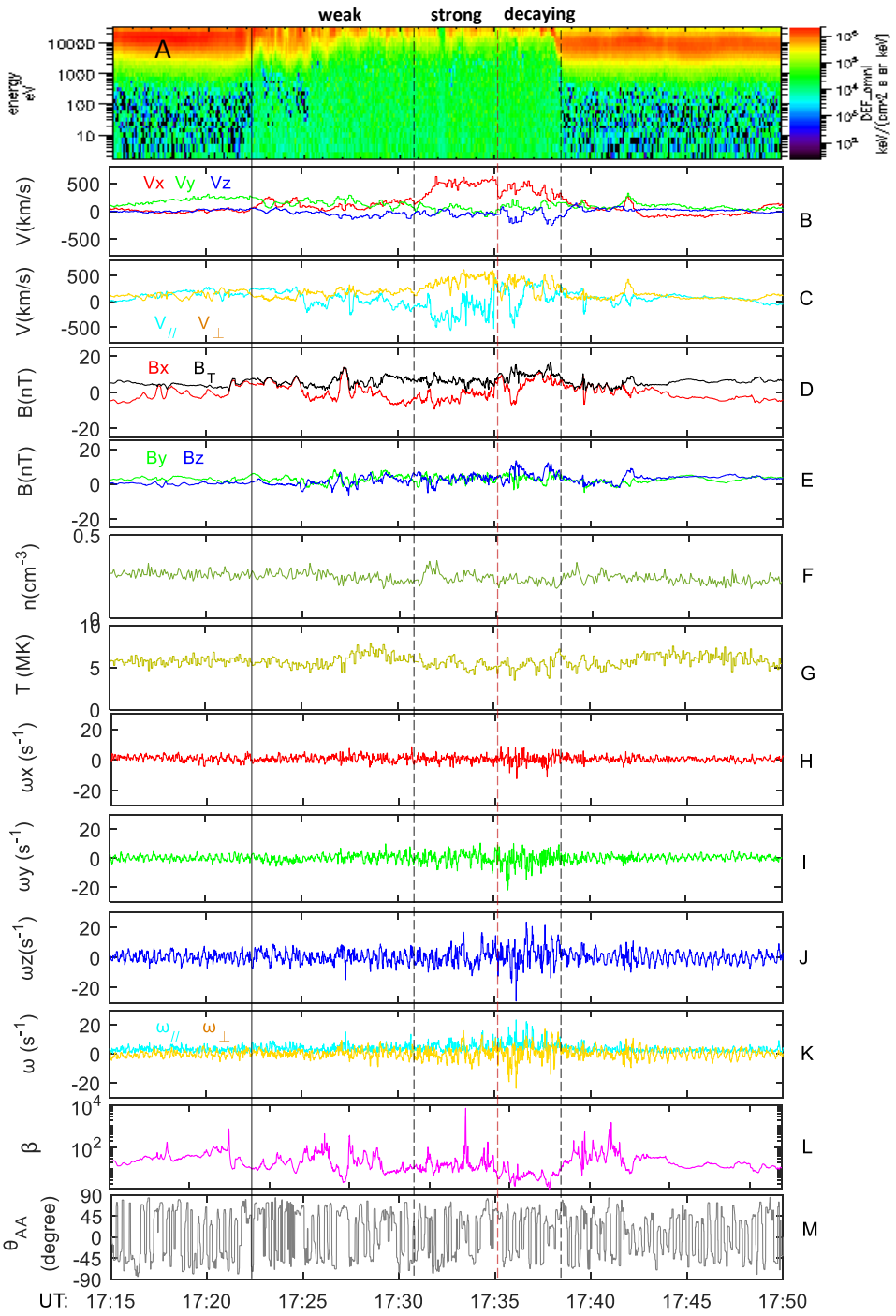

Figure 1. Evolutions of the vorticity field in the course of the reconnection jet on 26 July, 2017 MMS1 locates at (-23.4 R_E, 6.4 R_E, 4.4 R_E) (GSM). The BBF starts at 17:22 UT (solid vertical line), and ends at 17:37 UT (the last dashed line). Panel A is the ion energy flux spectrogram. Panel B plots the three components of the measured ion velocity. Panel C shows $V_{//}$ and $V_{\perp}$. Panels D and E are the measured Bx, By, Bz, and total B (B_T). Panels F to H are the all components of measured E and corresponding convective E (calculated by Ec= V×B). Panels I and J plot ωx, ωy, ωz, the total ω (ω_T). Panel K shows $\omega_{//}$ and $\omega_{\perp}$. Panel K shows the angel between V and B ($\theta_{VB} = \arctan(\frac{V_{\perp}}{V_{//}})$) and the anisotropic angle of the vorticity ($\theta_{AA} = \arctan(\frac{\omega_{\perp}}{\omega_{//}})$).

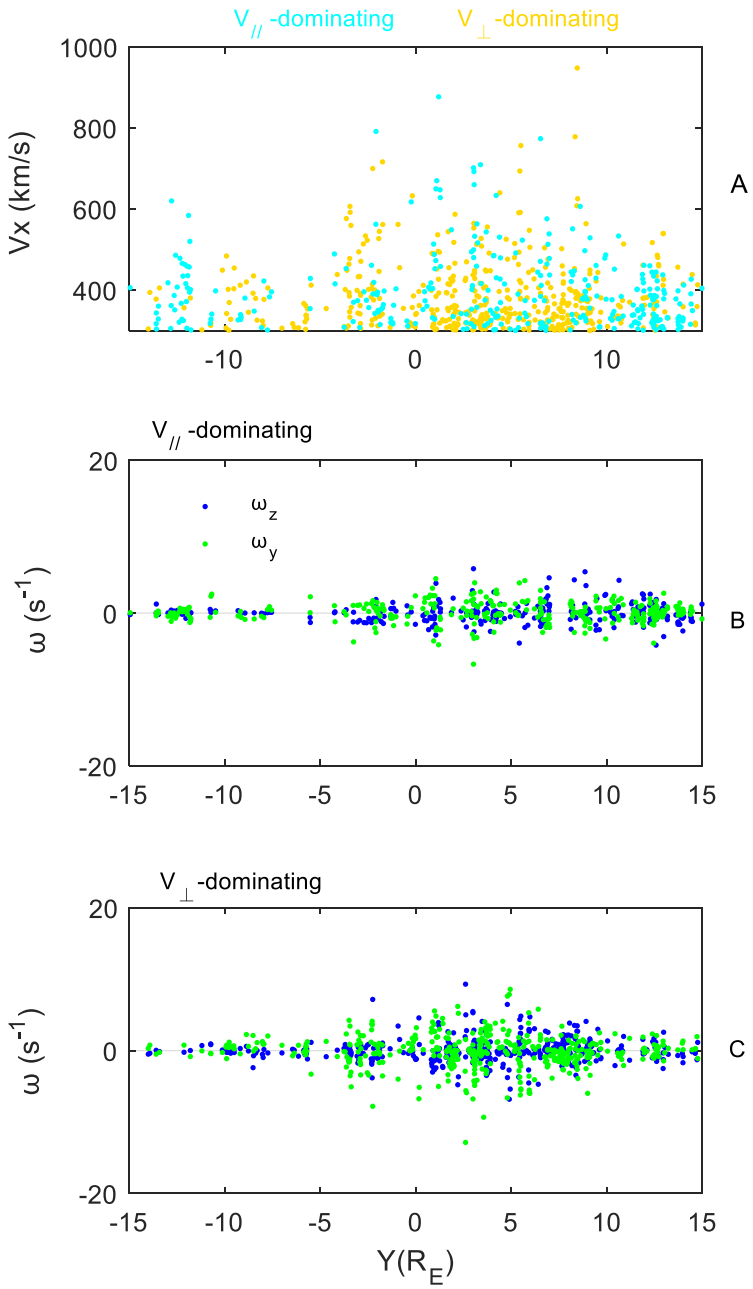

Figure 3. Scatter plots of the evolution of the vorticity field of the BBF in the dawn-dusk direction

Each point represents a BBF event. Panel A plots the BBF Vx. Panels B and C are the vorticity field in the $V_{//}$-dominating and $V_{\perp}$-dominating BBF, respectively.

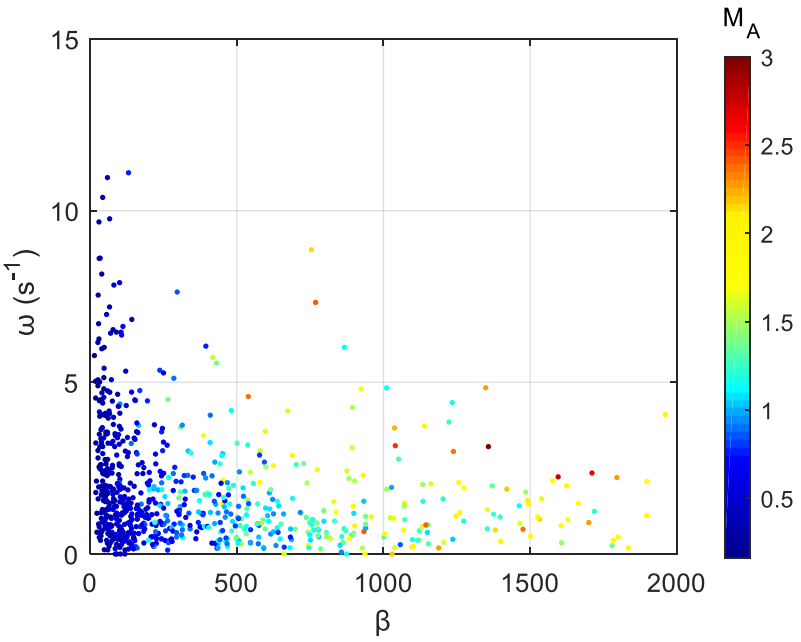

Figure 4. Scatter plot of β-dependence vorticity field of the BBF
Color of the point corresponds to the Alfvén Mach number $M_A = V/V_A$.

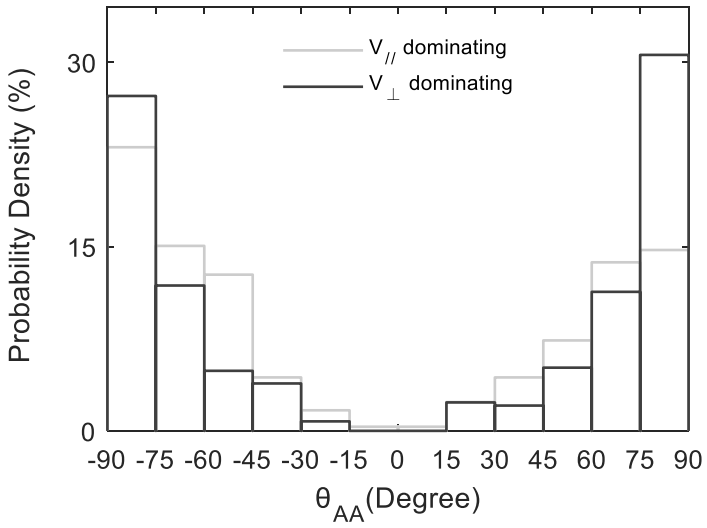

Figure 2. Probability densities of the θ_{AA} for the $V_{//}$-dominating and $V_{\perp}$-dominating BBF

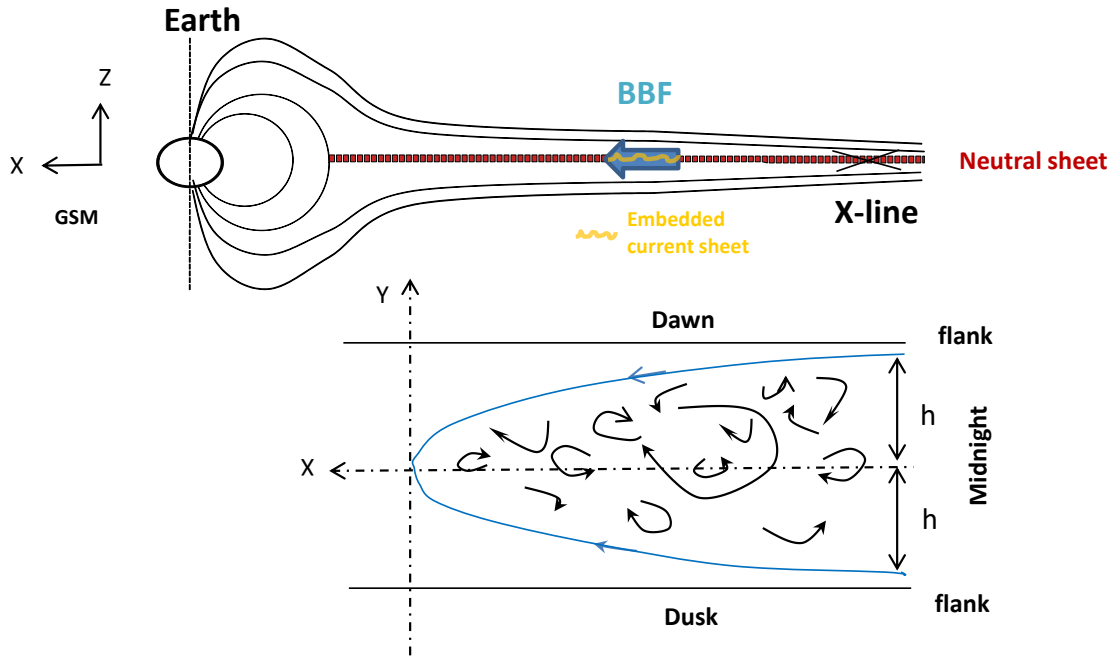

Figure 5. Cartoon of the vorticity field within the earthward traveling BBF embedded unsteady current sheet

The blue curved line with the arrow is the boundary of the reconnection jet. The vorticity field within the reconnection jet has significant dawn-dusk asymmetry.